Applied Physics B (2019) 125:90
https://doi.org/10.1007/s00340-019-7203-2

Applied Physics B
Lasers and Optics

Hydroxyl radical planar imaging in flames using femtosecond laser pulses

Yejun Wang[1] · Ayush Jain[1] · Waruna Kulatilaka[1]

Received: 7 January 2019 / Accepted: 25 April 2019 / Published online: 4 May 2019

Abstract
Hydroxyl radical (OH) planar laser-induced fluorescence (PLIF) imaging is one of the most widely used laser diagnostic techniques to investigate reacting flows such as flames and plasmas. In conventional PLIF experiments, 10-Hz, commercial Nd:YAG/dye-laser-based systems are often used for OH excitation. In recent years, significant developments are also reported in using diode-pumped solid-state and pulse-burst laser systems for high-repetition-rate (kHz–MHz) measurements. In general, all these laser sources generate nanosecond-duration, narrowband laser pulses which are to be tuned to a specific ro-vibrational excitation transition line. In the present work, we investigate the use of broadband, ultrashort femtosecond-duration (fs) laser pulses for OH-PLIF imaging in flames. The fs excitation of the OH $A^2\Sigma^+ \leftarrow X^2\prod$ (1, 0) transition is followed by fluorescence detection from the (0, 0) and (1, 1) vibrational bands. Because of the broad bandwidth, the excitation laser is coupled to a large number of OH ro-vibrational transitions at the same time; hence, species selectivity is obtained by detecting fluorescence emission in the 310–325 nm spectral window. This scheme is shown to be free from fluorescence from other flame species as confirmed by high-resolution fluorescence spectra recorded under a variety of flame conditions. Measured OH number density profiles in CH_4, C_2H_4 and H_2 calibration flames are in good agreement with model predictions. Two-dimensional imaging of OH at 1-kHz repetition rate is also demonstrated in a turbulent diffusion flame. The present fs OH-PLIF scheme can find novel applications in fundamental chemical physics research, as well as in practical engine combustion and flame diagnostics.

1 Introduction

The hydroxyl (OH) radical is considered to be a key intermediate species in chemical reactions involving hydrogen and hydrocarbon combustion. OH is a primary marker of the reaction zone and a key indicator of the heat release process in flames [1, 2]. Therefore, spatially and temporally resolved OH radical concentration data are critically important in fundamental and applied combustion and energy transfer studies. On the other hand, widespread implementation of laser-spectroscopy-based OH radical diagnostics is driven by its abundance in the reaction zone and the strong single-photon-allowed electronic transitions in the accessible ultraviolet (UV) wavelength region. Therefore, over the past four decades, considerable efforts have been devoted to OH laser-induced fluorescence (LIF) studies in numerous reacting flow systems such as flames and plasmas [2, 3]. Furthermore, because of its simple experimental configuration involving only one laser beam, aided by high fluorescence quantum yield, OH-LIF has been readily extended for two-dimensional (2D) planar LIF (PLIF) imaging [4–7], as well as 3D volumetric imaging in recent efforts [8, 9].

Several LIF excitation schemes involving (v', v'') vibrational bands of (0, 0) [10], (1, 0) [11], (2, 0), and (3, 0) [12] of the OH $A^2\Sigma^+ \leftarrow X^2\prod$ electronic manifold, have been explored for LIF measurements in reacting flows. For quantitative OH concentration measurements, non-radiative losses from laser-coupled upper energy levels, primarily via collisional quenching, must be accounted for. Most single-photon OH-LIF [11, 13] and two-photon OH-LIF [14–16] experiments are performed using nanosecond (ns) pulse duration (~ 10 ns, full width at half maximum, FWHM), Nd:YAG-based laser systems. The typical fluorescence lifetime of excited state OH radicals is in the order of 1–2 ns in atmospheric-pressure hydrocarbon flames [10], thus, excitation by ~ 10 ns FWHM laser pulses is insufficient for the

✉ Waruna Kulatilaka
waruna.kulatilaka@tamu.edu

[1] J. Mike Walker '66 Department of Mechanical Engineering, Texas A&M University, College Station, TX 77843-3123, USA

determination of time-resolved quenching rates. Moreover, most commercially available ns-duration lasers operate at low repetition rate, typically at 10 Hz, hence are incapable of capturing transient effects such as ignition-extinction dynamics and turbulent flow-flame interactions in practically relevant reacting flow conditions such as those present in gas turbine combustors [17]. In recent years, high-speed OH-LIF has also been performed in kHz-rate imaging using diode-pumped solid-state lasers coupled with high-speed dye lasers [1, 18], as well as custom-built, kHz–MHz-rate pulse-burst laser systems [8, 19]. However, the temporal duration of excitation laser pulses generally remain in the ns regime in all these approaches.

Ultrashort, broad bandwidth, picosecond [10, 20] or femtosecond (fs)-duration laser pulses are sufficiently short for nearly impulsive excitation and can enable in-situ determination of quenching rates. Fs excitation schemes have been demonstrated increasingly for efficient minor species measurements in recent years [21–24]. Additionally, the high-repetition-rate (i.e., 1–10 kHz) operation of these fs laser systems enables capturing the temporal evolution in certain unsteady flow environments [25]. On the other hand, in practically relevant high-pressure combustion environments, spectral line broadening, and shifting can significantly affect the excitation efficiency when ns-duration spectrally narrow laser pulses, typically on the order of 0.1 cm^{-1} are used [26, 27]. Broad spectral bandwidth, typically on the order of 300 cm^{-1} offered by fs-duration laser pulses can result in certain advantages in extending LIF diagnostics into high-pressure combustion environments [1, 28]. To the best of our knowledge, the only previously reported OH-LIF study using fs pulses involved two-photon excitation of the OH $A^2\Sigma^+ \leftarrow X^2\prod$ system [23]. In that work, for acceptable signal-to-noise ratio (SNR), single-point LIF signal collected using a photomultiplier tube (PMT) required a minimum of 512 laser shot averaging whereas recording dispersed fluorescence spectra required over 30,000 shot averaging. Averaging such a large number of shots was necessitated by the weak two-photon excitation efficiency, thereby hindering the single-shot 2D imaging warranted in many practical turbulent combustion studies.

In the present work, we investigate the application of broadband, fs-duration laser pulses for single-photon excitation of the OH $A^2\Sigma^+ \leftarrow X^2\prod$ system, and subsequent high-SNR, single-laser-shot, kHz-rate, 2D PLIF imaging in challenging reacting flow environments. The experimental details are presented in Sect. 2. The results and discussion in Sect. 3 include a detailed description of the broad bandwidth excitation-detection scheme and spectral selectivity issues in complex chemical environments as well as the effects of laser fluence. A subsequent discussion includes a comparison between experimental and calculated high-resolution emission spectra, followed by a range of measurements in H_2 and hydrocarbon flames along with flame simulations. Subsequently, 1-kHz 2D imaging demonstrations in a turbulent diffusion flame are presented revealing local flame structure and dynamics. The potential advantages and challenges of extension of the fs OH-PLIF scheme to elevated pressures are also discussed.

2 Experimental

The experimental apparatus consists of a regeneratively amplified Ti:Sapphire laser system (Spectra Physics, Model: Solstice Ace), generating approximately 80-fs-duration laser pulses at 1-kHz repetition rate. Approximately 6 mJ/pulse of the fundamental output beam at 800 nm was used to pump an optical parametric amplifier (OPA) (Light Conversion, Model: TOPAS Prime Plus with a NirUVis UV extension module) for generating UV radiation near 283 nm for exciting the $A^2\Sigma^+ \leftarrow X^2\prod$ (1, 0) transition of OH. The 283-nm output beam was directed through several 45° dielectric laser mirrors and focused onto the probe region using a + 200-mm focal-length plano-convex spherical lens. A thin, variable neutral density (ND) filter (Thorlabs, NDC-100C-4M) was placed before the lens to adjust the laser fluence reaching the probe region. The maximum 283-nm laser fluence available at the probe region was 0.71 J/cm^2.

Shown by the dotted lines in Fig. 1 is a typical spectrum of the excitation laser pulse obtained using a fiber-coupled miniature spectrometer (Ocean Optics, Model: Flame S) having a minimum wavelength resolution of 0.25 nm. The calculated OH-LIF excitation spectrum at 1-atm pressure and 2200-K temperature using the LIFBASE software package [29] is also shown in Fig. 1. For efficient excitation, a

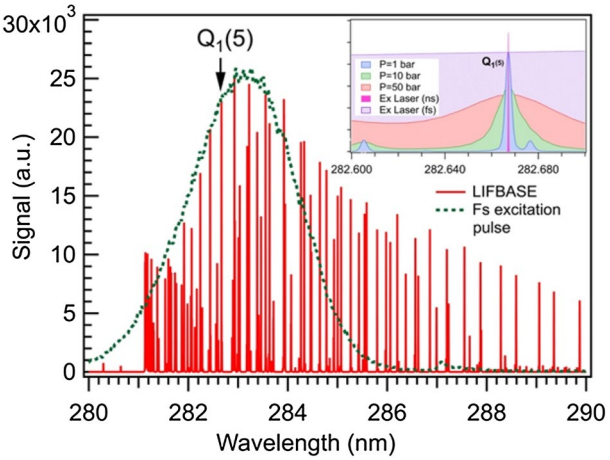

Fig. 1 A typical spectrum of the broadband excitation laser having approximately 80-fs pulse duration (dotted line), and the calculated OH-LIF excitation spectrum obtained at 2200 K and 1 atm using the LIFBASE software package [29] (color online)

typical narrowband ns excitation laser pulse should be centered on an individual ro-vibrational transition of the OH spectrum. For example, $Q_1(5)$ rotational transition of OH has a width on the order of 0.30 cm^{-1} (approximately 0.003 nm) at 1 atm and 2200 K, whereas the linewidth of a typical frequency-doubled narrowband output of an Nd:YAG-pumped dye laser is approximately 0.1 cm^{-1} FWHM. Hence, as shown by the inset in Fig. 1, extreme care has to be taken for optimal spectral overlap to enable efficient excitation and subsequent signal quantification when using ns pulses. In contrast, a broadband, 80-fs laser pulse excites a large number of ro-vibrational transitions covering approximately 250 cm^{-1} spectral range. As a result, effects of spectral broadening and shifting at elevated pressure become essentially insignificant in fs pulses, and typical spectral overlap corrections performed in ns excitation [26] become obsolete with the fs excitation.

However, broadband fs excitation essentially eliminates the spectral selectivity offered by a narrowband excitation laser pulse and risks exciting other fluorescing species within the laser linewidth. During this study, we show that such interferences are essentially non-existent in the case of OH-LIF as shown by the detailed emission spectroscopic studies performed in a variety of flame conditions. These results are described in detail in the following section. In addition, potential effects of temperature sensitivity of the excitation spectrum resulting from rotational redistribution in the wake of large temperature fluctuations are also discussed at the end.

For OH spectroscopic studies in flames, a 25.4 mm × 25.4 mm Hencken calibration burner was placed at the probe region. All measurements reported were performed at a height of 10 mm above the burner surface. The gas flow rates to the burner were regulated by calibrated mass flow controllers (MKS Instruments). The fluorescence signal was collected using a collimating lens placed orthogonal to the beam path and was transmitted to the entrance slit of a spectrometer (Princeton Instruments, Model: IsoPlane 320) using a fiber optic cable consisting of a circular-to-linear fiber array. The spectrometer has 150, 1200 and 2400 lines/mm gratings. The entrance slit width was set at 100 µm and an intensified CCD (ICCD) camera (Princeton Instruments, Model: PIMax4) was mounted at the exit plane of the spectrometer to record the spectra. The gate width and gain of the ICCD camera were set at 30 ns and 100%, respectively. The detection system was wavelength calibrated using a set of dual Hg and Ne–Ar calibration lamps (Princeton Instruments, Model: IntelliCal®). Subsequent OH-PLIF imaging at 1-kHz repetition rate was performed using a high-speed complementary metal-oxide semiconductor (CMOS) camera fitted with a high-speed image-relay optics (IRO) intensifier. The details of that apparatus are further discussed at the end.

3 Results and discussion

Shown in Fig. 2 is the OH fs-LIF signal as a function of the excitation wavelength. Spectra were recorded by scanning the excitation laser wavelength in steps of 1 nm in a $\Phi = 1.0$ CH_4/air flame. The values shown are the center wavelengths of the broadband fs laser pulse at each step. For this case, the excitation laser fluence was fixed at 0.26 J/cm^2, and the fluorescence signal was averaged for 30 camera frames with 600 laser shot on CCD accumulations in each frame. It is observed that the excitation wavelength centered around 283 nm results in the maximum LIF signal. The shape of the experimentally obtained LIF excitation spectrum is well predicted by a LIFBASE [29] simulated spectrum at 1-atm pressure, with the assumption of vibrational nonequilibrium as discussed in detail with respect to the spectral fitting in Fig. 3. To account for the spectral broadening by the broadband excitation laser pulse, a 2.2-nm instrument resolution (corresponding to the bandwidth of the excitation laser pulse shown in Fig. 1) was used during the LIFBASE simulation.

When broadband fs excitation is used, species selectivity can often be evaluated by the spectrally resolved fluorescence emission signal. Shown in Fig. 3 are the high-resolution spectra of the (0, 0) + (1, 1) and (1, 0) emission bands of OH obtained in a stoichiometric CH_4/air flame, recorded using the 2400 lines/mm spectrometer grating. The laser fluence was fixed at 0.26 J/cm^2. In both cases, the experimental spectra agree within ± 5% of the calculated OH spectra at 1 atm pressure, using the LIFBASE software package assuming an instrument resolution of 0.08 nm. Potential sources for this moderate mismatch, explained in terms of the rotational and vibrational thermalization

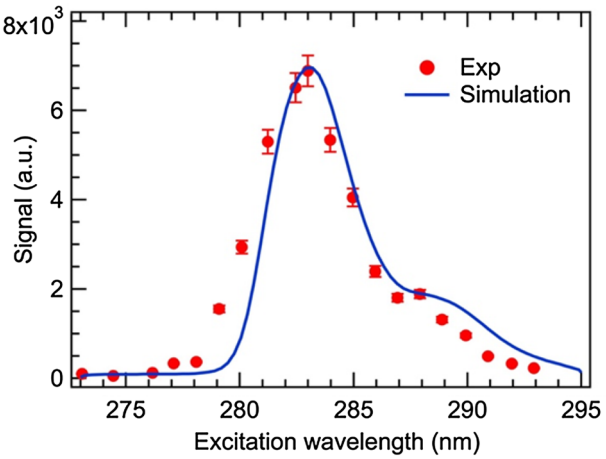

Fig. 2 Dependence of the fs OH-LIF signal on the excitation wavelength. Simulation was performed using the LIFBASE [29] at $T = 2236$ K and $P = 1$ atm, with the assumption of vibrational nonequilibrium (color online)

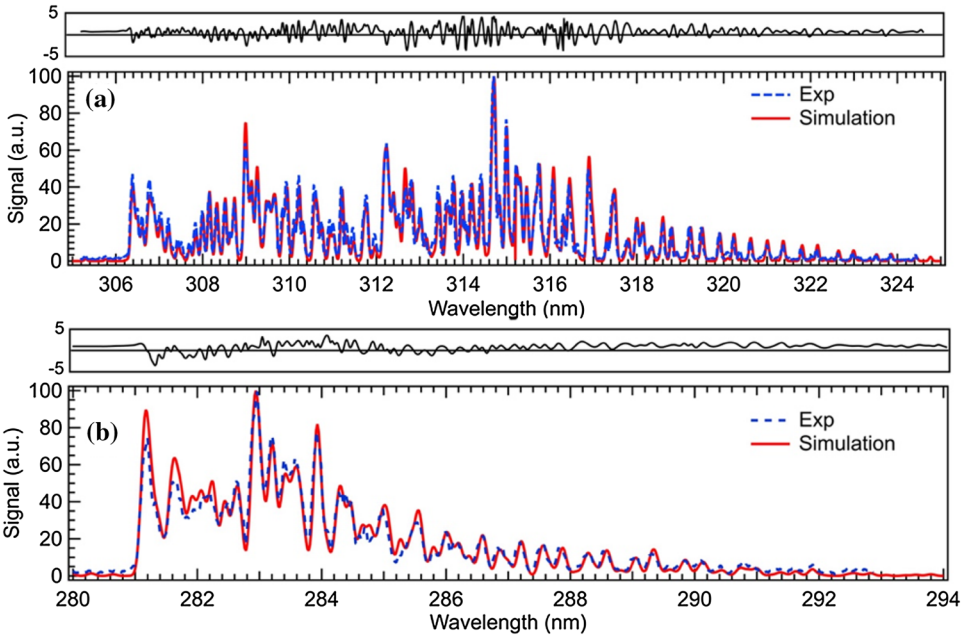

Fig. 3 Comparison of fs-LIF emission spectra of the OH (0, 0) + (1, 1) bands (**a**), and OH (1, 0) band (**b**) in a stoichiometric CH_4/air flame. Simulated spectra were calculated using the LIFBASE [29] as described in the text (color online)

effects during the fs-duration excitation laser pulse are further described in the next paragraph. The OH (0, 0) + (1, 0) experimental spectrum was background corrected by simply subtracting the signal recorded by blocking the excitation laser beam. However, the OH (1, 0) raw spectrum contained a significant contribution from the scattered excitation laser light, hence, a scaled laser spectrum recorded in room air was subtracted from the raw spectrum. The scaling factor was adjusted until the optimum least squares fit was obtained.

When calculating the theoretical spectrum, the rotational temperature was set at 2200 K, which is close to the expected adiabatic flame temperature. However, to obtain the best fit, vibrational nonequilibrium has to be assumed. At 2200 K, the equilibrium vibrational population distribution fractions in the upper state for $v' = 0$, 1 and 2 is 90.2, 8.7 and 1.0%, respectively. However, in the best fit spectra shown in Fig. 3, the resulting vibrational population distribution for $v' = 0$, 1 and 2 is 33.1, 66.8 and 0.1%, respectively. The latter corresponds to an approximately 60% less population transfer to the $v' = 0$ level through vibrational energy transfer (VET) collisions, while 66.8% of the upper state population remains in the directly laser-coupled $v' = 1$ excited state. In traditionally used approximately 10-ns-duration excitation laser pulses, the fluorescence emission generally agrees well with Boltzmann statistics where the excited-state population distribution is assumed fully thermalized. In the present scheme using fs excitation pulses, the above observation suggests non-thermalized population distribution of the excited state during the time scale of fluorescence emission. These observations and potential follow-on investigations are further discussed at the end of this section.

The laser fluence dependence of the fs OH-LIF signal was investigated by plotting the integrated signal in the 305–325 nm spectral window as a function of the laser fluence. The results are shown in Fig. 4. The error bars shown are 2-sigma standard deviations of the four repeated measurements. The focusing lens used was + 200 mm, corresponding to a beam waist of 80 µm, estimated using a UV beam profiling camera. As shown in Fig. 4, the OH-LIF signal scales linearly with laser fluence for values below approximately 0.26 J/cm^2 and exhibits partial saturation beyond this value. Hence, during all subsequent experiments, the laser fluence was fixed at 0.2 J/cm^2 to ensure the measurements were performed in the linear LIF region.

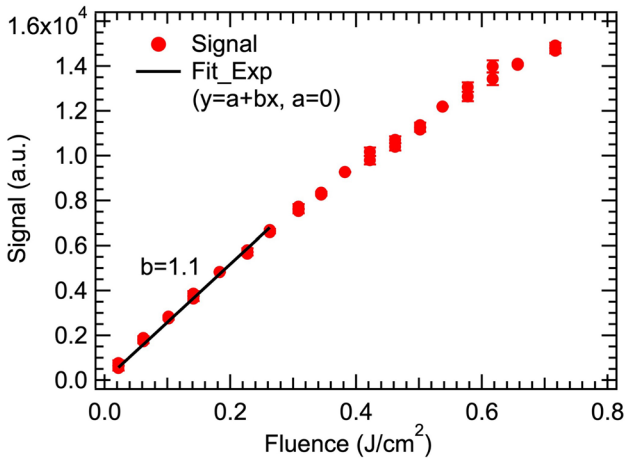

Fig. 4 Laser fluence dependence of OH fs-LIF signal recorded in a stoichiometric CH_4/air flame. The estimated beam waist is approximately 80 µm (color online)

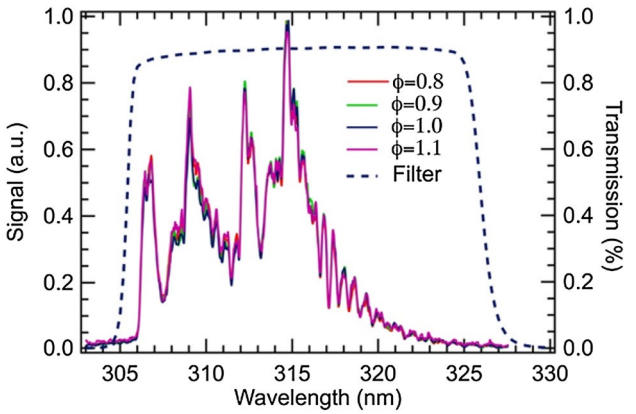

Fig. 5 Peak-normalized OH-LIF emission spectra recorded for four different equivalence ratios of CH_4/air flame. The transmission spectrum of the fluorescence detection filter used for subsequent imaging studies is also shown by the dashed line (color online)

As seen in Fig. 4, the slight tilt observed beyond the pulse energy of 0.26 J/cm^2 may be an indication of partial saturation of the transition, although other effects such as ionization can become significant at high pulse energies.

To explore possible fluorescence interferences that may result from the broadband excitation, OH-LIF spectra were recorded in a series of CH_4/air flames while varying the equivalence ratio (Φ) from lean to rich. Figure 5 shows the peak-normalized fluorescence spectra of OH (0, 0) + (1, 1) bands from such flames recorded using the 1200 lines/mm grating in the spectrometer. Under these conditions, the manufacturer-specified instrument resolution for the spectrometer/ICCD camera system is approximately 0.3 nm/pixel, which also agrees with that of the simulated LIF spectrum (not shown) in similar conditions. It is seen that the spectra are nearly identical in flames for all equivalence ratios investigated, indicating no evidence of spectral interferences, especially in rich hydrocarbon flames. Spectra recorded at other flame conditions reported in the following section are also found to have the same general shape. These results suggest that a broadband fluorescence detection scheme similar to that followed using narrowband ns excitation can still be used with the broadband fs excitation scheme in these flames. Therefore, a 15-nm-wide fluorescence detection filter (Semrock, Model FF01-315/15) represented by the transmission curve shown by the dash line in Fig. 5 was incorporated for all subsequent imaging experiments.

To further verify the applicability of the fs-LIF scheme, OH concentration profiles were obtained in a range of CH_4/air, C_2H_4/air and H_2/air laminar flames stabilized over the Hencken calibration burner. To obtain stable flames, the total flow rates of CH_4/air and C_2H_4/air flames were maintained at 10 slm (standard liters per minute), and the Φ was varied between 0.7–1.5 and 0.5–1.5, respectively, by adjusting the relative fuel/air ratio. N_2 shroud gas was used to stabilize the flames by minimizing shear perturbations with the surrounding air. For H_2/air flames, the air flow rate was fixed at 52 slm and the H_2 flow rate was varied between 15 and 35 slm to obtain the range Φ between 0.7 and 1.6. At each flame condition, OH-LIF spectra similar to those shown in Fig. 5 were recorded and by direct comparison, it was ensured no spectral interferences were present. The integrated OH-LIF signals as a function of Φ are shown in Fig. 6. The equilibrium OH mole fractions were calculated using CANTERA [30] chemical equilibrium codes and were converted to number densities using the equilibrium flame temperature obtained using CANTERA. Based on the equilibrium mole fractions, the variation of the overall quenching rate can vary between 10 and 80%. However, no quenching

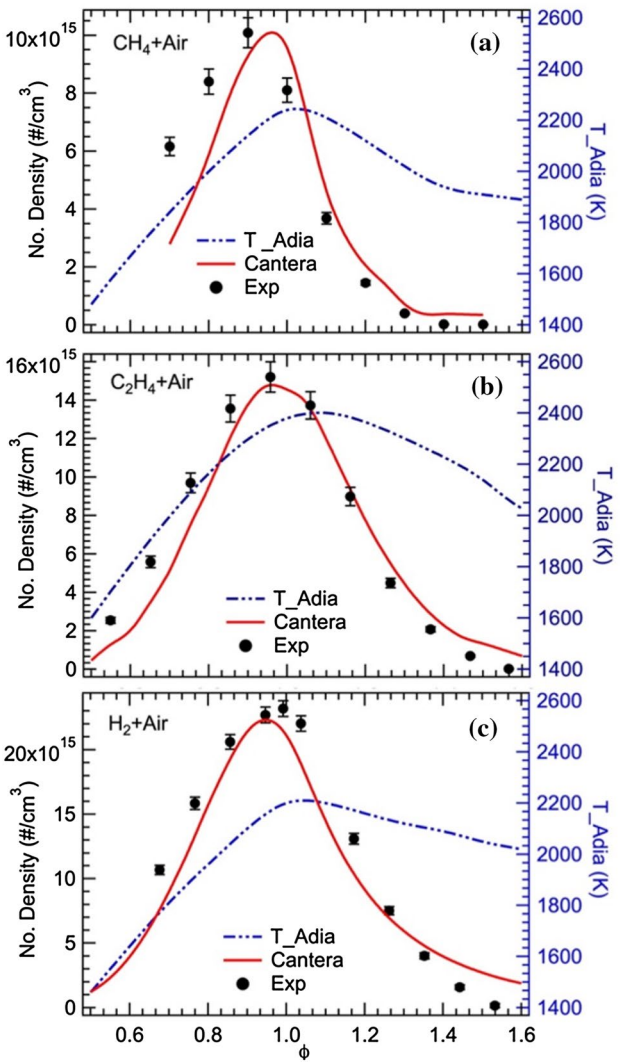

Fig. 6 Fs-LIF signal of OH as a function of equivalence ratio in **a** CH_4/air, **b** C_2H_4/air and **c** H_2/air flames stabilized over the Hencken calibration burner (color online)

corrections were applied to the measured LIF signals, and the shape of the relative OH-LIF signal intensity is directly compared with the calculated OH number density values. At each equivalence ratio, 600 laser-shot on CCD accumulations were used and 10 frames were averaged. The estimated 2-sigma error bars from the 10 frames are also shown for each data point in Fig. 6.

It can be seen that the calculated equilibrium OH profiles are well predicted for all three fuel cases investigated. The OH concentration increases with increasing Φ up to near stoichiometric conditions and then decreases as the flames become rich and the flame temperatures drop. On the fuel-lean side of all flames, the measured OH number densities are underpredicted by equilibrium calculations. This observation may result from a combination of experimental uncertainties in flow rate measurements as well as deviations from equilibrium assumptions in real flames. Overall, the fs-LIF scheme is proven to be an effective method for OH concentration measurements in these flame conditions.

Experimentally, measured fs OH-LIF profiles in the C_2H_4/air flames under the identical flame conditions are also compared with previously reported ns OH-LIF data as well as numerically calculated OH profiles as a function of the height above the burner (HAB) [31]. These comparisons are shown in Fig. 7. The calculated OH profiles were generated from a well-validated, time-dependent, axisymmetric CFD code UNICORN (unsteady ignition and combustion using reactions) which includes detailed chemical kinetics. As can be seen in the top panel of Fig. 7, for locations near the burner surface such as HAB = 5 mm, both ns and fs OH-LIF profiles deviate from the calculated values for all equivalence ratios, although the fs OH-LIF measurements show improved match on the fuel-rich flames. The overall mismatch near the burner surface may result from spatial averaging effects of the measurements over the diffusion flamelets present near the burner surface of the Hencken burner [32]. However, at HAB = 10 and 20 mm locations, fs-LIF profiles match well with code predictions reported in Ref. [31]. The flame is expected to be nearly uniform in these HAB locations. These improved agreements also demonstrate that the fs-LIF technique is an effective method for OH concentration measurements in a wide range of flame conditions. It should also be noted that equilibrium flame temperatures vary by approximately 800 K over the different flame conditions reported in Figs. 6 and 7, nevertheless, fs OH-LIF results are generally in good agreement with model predictions. We expect the improved agreement may have resulted in part by the broadband excitation laser pulse encompassing a large number of rotational states making it less sensitive to rotational redistributions when the flame temperature varies over a wide range. A LIFBASE simulation in the temperature range of 1600–2400 K indicates a negligible change in spectral overlap fraction when all

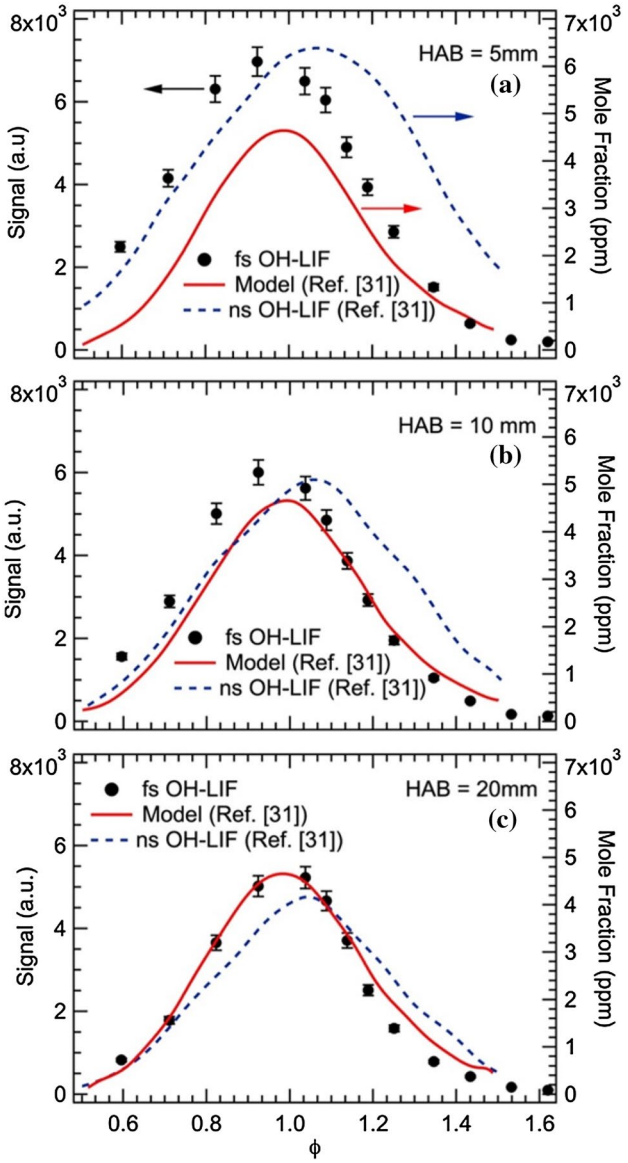

Fig. 7 Comparison of fs OH profiles with previously reported ns OH profiles and model predictions [31] at different heights in C_2H_4/air flames (color online)

rotational states under the bandwidth of the fs excitation pulse are considered.

Finally, the fs excitation scheme was extended for 2D, OH planar LIF (PLIF) imaging measurements in a turbulent diffusion flame. For PLIF measurements, the $f = +200$ mm plano-convex lens was replaced by a $f = +100$ mm plano-convex lens, followed by a $f = -25$ mm cylindrical lens, thereby generating a laser sheet having an effective height of approximately 15 mm near the focal region. The flame used for OH-PLIF studies was a diffusion CH_4/H_2 (1:1) jet with a total flow rate of 24 slpm through a 4.5-mm diameter central tube. The corresponding Reynolds number at the jet exit is approximately 3000. The central jet is surrounded

by an annular region of 50.8-mm diameter consisting of an air co-flow. A high-speed CMOS camera (Photron, Model: SA-Z) coupled with a high-speed IRO intensifier (LaVision, Model: HS-IRO) was used to record fs OH-PLIF images of the diffusion flame near the nozzle exit. The intensifier was operated in the linear response regime by maintaining the gain setting below 70% as confirmed through previous similar experiments. A 45-mm-focal-length $f/1.8$ UV camera lens was used to collect the fluorescence signal, along with the bandpass filter depicted by the dash line in Fig. 5. In addition, spectrally resolved fluorescence signals were also recorded in these flames and was confirmed that it is nearly identical to the interference-free LIF signal similar to those shown in Fig. 5. An illustrative set of OH-PLIF images from a 1-kHz image sequence is shown in Fig. 8, along with a photograph of the turbulent diffusion flame in the first panel. The OH-PLIF signal is zero in the central core where the cold fuel is present and reaches the maximum value at the two flame fronts where the fuel is entrained by surrounding oxidizer. The SNR of the single-shot PLIF images was determined as the ratio of the mean value of the signal and the standard deviation of the signal over a 32-pixel × 32-pixel square, corresponding to an approximately 0.8 µm × 0.8 µm region at the flame front. The peak SNR is estimated to be approximately 40, which is comparable to that reported in most ns OH-PLIF experiments [5, 33, 34]. Flame wrinkling due to turbulent flow is well captured in this 1-kHz image sequence. Furthermore, in the bottom panel, a localized extinction and subsequent re-ignition event can be observed by the right side of the flame.

Better understanding of the non-radiative fluorescence quenching process following ultrashort-pulse fs excitation scheme will require a dedicated study follow-on considering rotational energy transfer (RET), VET and quenching rates. However, several general observations can be made based on the present results. Quenching and VET rates typically occur at similar time scales and are much slower than characteristic RET rates [35]. As outlined above, we observe a non-thermalized vibrational population redistribution during the fluorescence emission following a fs excitation pulse. Approximately, 60% less population transfer to the $v'=0$ level through vibrational energy transfer (VET) collisions suggests reduced VET rates during fs-LIF emission as compared to fully thermalized Boltzmann population distribution in the upper electronic manifold during typical ns LIF excitation timescales. Since fluorescence quenching takes place at similar timescales as VET it can be assumed fs-LIF scheme may be less susceptible for fluorescence quenching, a hypothesis which may be tested and quantified using a pump-probe study [36] and/or a carefully designed time-gated fluorescence detection scheme during future investigations. Such measurements can be incorporated into a detailed VET study involving a comprehensive rate-equation model [37–39] to further investigate time-dependent broadband excitation dynamics of fs pulses on the entire ro-vibrational manifold. In addition, when fs pulses propagate through thick optical media such as windows, the resulting temporal and spatial distortions will need to be investigated in detail to extend the present diagnostic approach to high-pressure combustion media. Such challenges are common to all ultrafast laser-based diagnostic techniques, and related mitigation strategies are an active area of research by many groups.

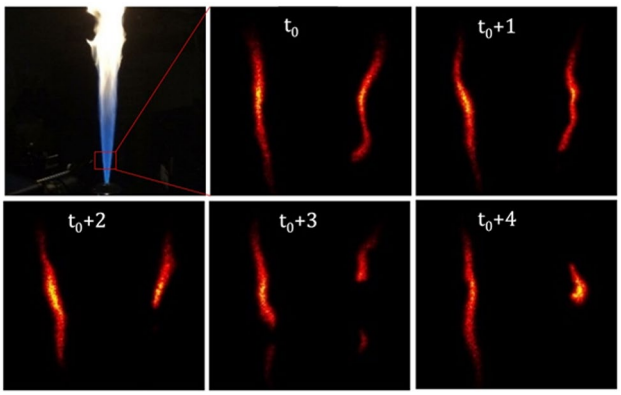

Fig. 8 Consecutive single-laser-shot OH-PLIF images recorded at a pulse repetition rate of 1 kHz in a diffusion CH_4/H_2 (1:1) jet flame. Jet exit Reynolds number is approx. 3000. Each frame corresponds to an area of 16 mm × 16 mm

4 Conclusions

In this work, we have demonstrated for the first time, the application of the broadband, ultrashort fs-duration laser pulses for OH-PLIF imaging in flames. Species selectivity is confirmed by observing the spectrally resolved emission signals, which agree well with the calculated OH spectra. A linear dependence of the OH-LIF signal on the laser fluence was observed below 0.26 J/cm^2 while partial saturation was present at higher laser fluences. Measured OH fluorescence signals are well predicted by the calculated equilibrium OH number densities in CH_4, C_2H_4, and H_2 flames over a wide range of flame equivalence ratios. Additionally, an improved agreement was obtained between measured and calculated OH profiles at different locations above the burner surface for C_2H_4/air flames stabilized over the Hencken calibration burner. High-SNR, 1-kHz, single-laser-shot fs OH-PLIF imaging was also demonstrated in a turbulent CH_4/H_2 diffusion flame. The implications of ultrashort-pulse broadband excitation scheme for OH-LIF detection in terms of excitation dynamics and different energy transfer processes are discussed, and the potential applications for elevated-pressure environments with steep thermal gradients are outlined.

Overall, fs pulse excitation scheme is a promising method for OH-PLIF detection in a range of practical reacting flow environments as well as forming a basic foundation for excitation dynamics and fundamental energy transfer studies under controlled laboratory conditions.

Acknowledgements Funding support from the National Science Foundation (NSF) (Contract No. CBET-1604633), and the Office of Naval Research (ONR) (Contract No. N00014-16-1-2578).

References

1. I. Boxx, C. Slabaugh, P. Kutne, R.P. Lucht, W. Meier, Proc. Combust. Inst. **35**, 793 (2015)
2. A.C. Eckbreth, *Laser Diagnostics for Combustion Temperature and Species* (CRC Press, Boca Raton, 1996), p. 630
3. J.W. Daily, Prog. Energy Combust. Sci. **23**, 133 (1997)
4. J.R. Osborne, S.A. Ramji, C.D. Carter, S. Peltier, S. Hammack, T. Lee, A.M. Steinberg, Exp. Fluids **57**, 57 (2016)
5. W.D. Kulatilaka, P.S. Hsu, J.R. Gord, S. Roy, Opt. Lett. **36**, 1818 (2011)
6. J. Kiefer, Z.S. Li, J. Zetterberg, X.S. Bai, M. Aldén, Combust. Flame **154**, 802 (2008)
7. M.J. Dyer, D.R. Crosley, Opt. Lett. **7**, 382 (1982)
8. B.R. Halls, P.S. Hsu, N. Jiang, E.S. Legge, J.J. Felver, M.N. Slipchenko, S. Roy, T.R. Meyer, J.R. Gord, Optica **4**, 897 (2017)
9. W. Cai, X. Li, L. Ma, Appl. Opt. **52**, 8106 (2013)
10. M. Jonsson, A. Ehn, M. Christensen, M. Alden, J. Bood, Appl. Phys. B Lasers Opt. **115**, 35 (2014)
11. J.H. Frank, S.A. Kaiser, M.B. Long, Proc. Combust. Inst. **29**, 687 (2002)
12. K.L. Steffens, J. Luque, J.B. Jeffries, D.R. Crosley, J. Chem. Phys. **106**, 6262 (1997)
13. A. Matynia, M. Idir, J. Molet, C. Roche, S. de Persis, L. Pillier, Appl. Phys. B **108**, 393 (2012)
14. J. Kojima, Q.-V. Nguyen, Phys. Lett. **396**, 323 (2004)
15. J.E.M. Goldsmith, N.M. Laurendeau, Appl. Opt. **25**, 276 (1986)
16. D.R. Crosley, G.P. Smith, J. Chem. Phys. **79**, 4764 (1983)
17. R. Borghi, S.N.B. Murthy, (Springer, New York, 1989)
18. L. Ma, Q. Lei, T. Capil, S.D. Hammack, C.D. Carter, Opt. Lett. **42**, 267 (2017)
19. B. Thurow, N. Jiang, W. Lempert, Meas. Sci. Technol. **24**, 1 (2013)
20. T.B. Settersten, A. Dreizler, R.L. Farrow, J. Chem. Phys. **117**, 3173 (2002)
21. W.D. Kulatilaka, J.R. Gord, V.R. Katta, S. Roy, Opt. Lett. **37**, 3051 (2012)
22. W.D. Kulatilaka, S. Roy, N. Jiang, J.R. Gord, Appl. Phys. B **122**, 1 (2016)
23. H.U. Stauffer, W.D. Kulatilaka, J.R. Gord, S. Roy, Opt. Lett. **36**, 1776 (2011)
24. Y. Wang, W.D. Kulatilaka, Appl. Phys. B **124**, 1 (2018)
25. Y. Wang, C. Capps, W.D. Kulatilaka, Opt. Lett. **42**, 711 (2017)
26. S.V. Naik, N.M. Laurendeau, Appl. Phys. B **79**, 641 (2004)
27. O. Carrivain, M. Orain, N. Dorval, C. Morin, G. Legros, Appl. Spectrosc. **71**, 2353 (2017)
28. S. Candel, G. Singla, P. Scouflaire, C. Rolon, L. Vingert, J. Propuls. Power **23**, 593 (2007)
29. J. Luque, D.R. Crosley, SRI International Report MP 99-009 (1999)
30. D.G. Goodwin, H.K. Moffat, R.L. Speth, Version 2.3.0 (2017), http://www.cantera.org
31. T.R. Meyer, S. Roy, T.N. Anderson, J.D. Miller, V.R. Katta, R.P. Lucht, J.R. Gord, Appl. Opt. Opt. **44**, 6729 (2005)
32. W.D. Kulatilaka, R.P. Lucht, S.F. Hanna, V.R. Katta, Combust. Flame **137**, 523 (2004)
33. U. Retzer, R. Pan, T. Werblinski, F.J. Huber, M.N. Slipchenko, T.R. Meyer, L. Zigan, S. Will, Opt. Exp. **26**, 18105 (2018)
34. Z. Wang, P. Stamatoglou, Z. Li, M. Alden, M. Richter, Opt. Exp. **25**, 30214 (2017)
35. P. Beaud, P.P. Radi, D. Franzke, H.-M. Frey, B. Mischler, A.-P. Tzannis, T. Gerber, Appl. Opt. **37**, 3354 (1998)
36. X. Chen, T.B. Settersten, Appl. Opt. **46**, 3911 (2007)
37. R. Kienle, M.P. Lee, K. Kohse-Höinghaus, Appl. Phys. B **62**, 583 (1996)
38. P.H. Paul, J.L. Durant, J.A. Gray, M.R. Furlanetto, J. Chem. Phys. **102**, 8378 (1995)
39. U. Rahmann, W. Kreutner, K. Kohse-Höinghaus, Appl. Phys. B **69**, 61 (1999)